Supplementary Material

Mechanical Detection of Dipole-Dipole Interactions between Electronic Spins in a Solid

C. Pellet-Mary, P. Huillery, M. Perdriat, G. Hétet

[1] *Laboratoire de Physique de l'Ecole normale supérieure, ENS, Université PSL, CNRS, Sorbonne Université, Université Paris-Diderot, Sorbonne Paris Cité, Paris, France.*

Contents

I. NV$^-$ CENTER THEORY

A. NV spin Hamiltonian

The NV spin Hamiltonian in its fundamental level can be written as :

$$\hat{\mathcal{H}}_s = DS_z^2 + \gamma_e \mathbf{B} \cdot \hat{\mathbf{S}},$$

Where $D = (2\pi)2.87$ GHz is the crystal field splitting originating from a spin-spin interaction, and $\gamma_e = 28$GHz/T is the electron gyromagnetic ratio. We neglected contributions of the strain and local electric field since we are working with magnetic fields of the order of 100G, as well as the hyper-fine interaction with ^{14}N since we are working with ensembles with a typical inhomogeneous broadening $\frac{1}{T_2^*} \approx (2\pi)5$ MHz.

The $\mathbf{z}$ axis of the S_z operator here is the axis formed by the nitrogen atom and the vacancy, hence why we do have different energy transitions for different NV orientations, depending on the projection of the magnetic field on the NV axis.

B. Diamond crystalline axes and degeneracy conditions

There are four possible crystalline axis for the NV centers (so-called "classes" of NV) which are depicted in Fig. 1 b) and correspond to the crystalline directions [111], [$1\bar{1}\bar{1}$], [$\bar{1}1\bar{1}$] and [$\bar{1}\bar{1}1$].

The magnetic field is represented in the diamond basis in Fig. 1 a) where the usual polar and azimuthal angles θ and ϕ are defined with respect to the $\mathbf{z}$ ([001]) direction.

For some orientations of the magnetic field, the projection of the magnetic field on two or more NV axes will be identical, and therefore the energy level of the corresponding classes will be the same. These degeneracies are represented on fig 1 c), where the dashed lines are the locus of the crystalline planes orthogonal to the [110] directions (6 planes in total). When the magnetic field belongs to these plane, we observe a degeneracy between two classes of NV, as can be seen in the Fig. 4 of the main paper.

The plain lines are the locus of the planes orthogonal to the [100] directions (3 planes total). When the magnetic field is in these planes, every class is at resonance with another class, as can be seen in Fig. 6.

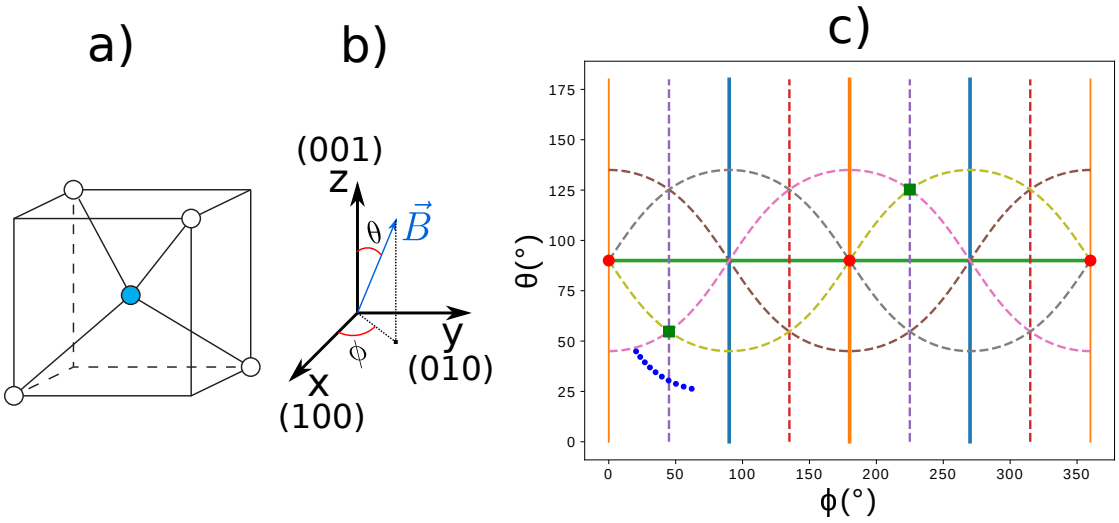

FIG. 1: a) Representation of the four crystalline axes of the diamond b) Representation of the magnetic field in the diamond crystalline basis c) Representation in the (θ, ϕ) basis of the crystalline planes ($[110]_\perp$ family of planes in dashed lines, $[100]_\perp$ in plain lines), [100] direction as a red circles, [111] direction as a green squares and the path of the magnetic field in the experiment of Fig. 3 of the main text in blue dots.

The red circles correspond to the [100] directions, for which the four classes of NV or at degeneracy, and the green squares to the [111] direction where one class is aligned with the magnetic field, and the three other are at degeneracy.

Finally the blue dots correspond to the path followed by the magnetic field in the experiment presented in Fig 3. of the main text, where we can see a degeneracy plane of the $[110]_\perp$ family being crossed.

II. EXPERIMENTAL DETAILS

A. Experimental setup

The experimental setup illustrated in Fig.2 is very similar to the one used in [1] with the addition of a permanent magnet and an electromagnetic (EM) coil in order to perform magnetic field scans. The diamond sample is typically illuminated with 1mW of 532 nm laser light, focused by a NA = 0.5 objective. An acousto-optic modulator (AOM) is used to switch on and off the 532nm laser and to finely tuned its power. The photo-luminescence

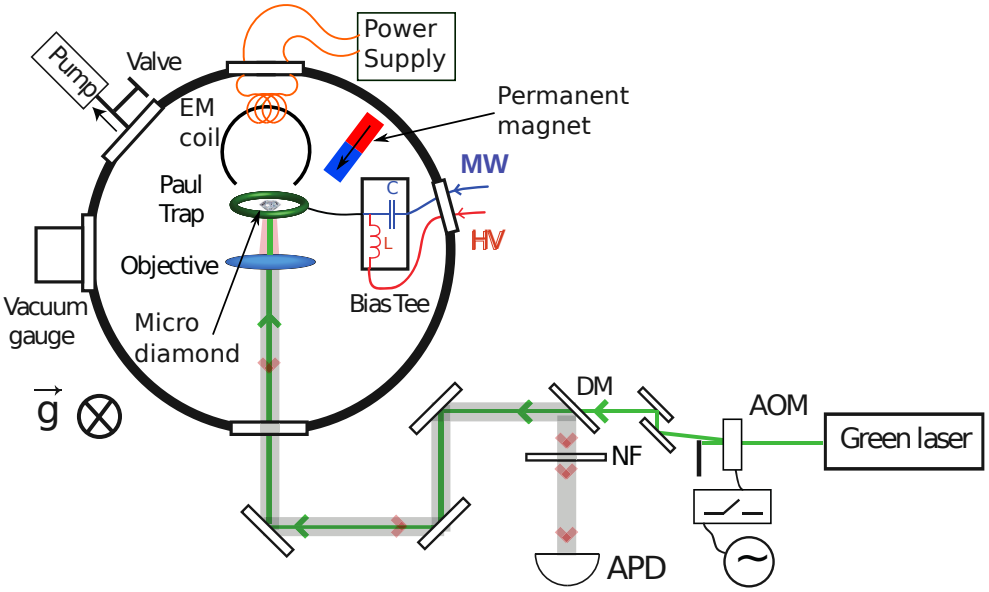

FIG. 2: Illustration of the experimental setup

(PL) is collected by the objective, separated form the excitation light using a dichroic mirror (DM) and a 532nm notch filter (NF), and detected using a multimode-fibered single-photon avalanche photo-detector (APD) (SPCM-AQRH-15 from Perkin Elmer). Typically, we detect PL photons at a rate of 1 MHz.

The Paul trap is a pseudo-ring with a diameter of approximately 200 μm, as can be seen in [2]. It acts both as trap through the high voltage (HV) and as a microwave (MW) antenna.

The magnetic field generated by the (homemade) EM coil is controlled by a programmable power supply (Rhode & Shwartz NGE 103) performing current ramps.

While the levitating setup is located in a vacuum chamber, all the experiments presented in this article are performed at atmospheric pressure.

B. T_1 Measurement

The protocol to measure the spin lifetime of the NV centers, as presented in Fig 2. of the main text, is described in Fig. 3 . In the first sequence the spins are initially polarized in their $m_s = |0\rangle$ state through a 1 ms green laser excitation pulse and then left to evolve in the dark for a variable dark time τ. The spin state is finally read out with a 10 μs laser pulse, shorter than the polarization time of the spins.

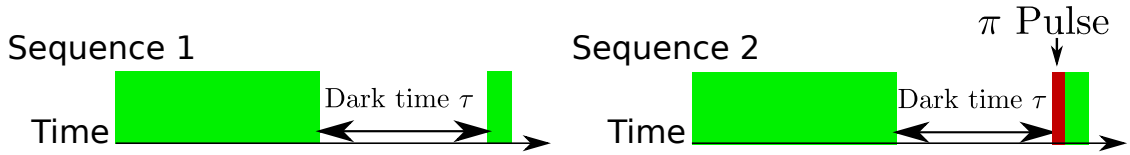

FIG. 3: T_1 measurement protocol for a single class in an ensemble of NV centers. Green bars represent laser excitation, red bar represent microwave π pulse for the selected class

The second sequence uses the same parameters (polarization time, dark time and readout time) than the first sequence but adds a resonant microwave π pulse on a transition of one of the four classes of NV^- right before the readout pulse, exchanging the population of the $m_s = |0\rangle$ state with one of the $m_s = |\pm 1\rangle$ state.

Noting S_1 the signal given by the first sequence and S_2 the one given by the second sequence, then by looking at $S_1 - S_2$ we can measure the spin state population of a single class, and remove unwanted contributions to the photoluminescence, such as charge state transfer in the dark (which would be common to the two signals and therefore subtracted). In order to avoid low frequency noises or drift, we alternate both sequence when performing the measurement.

C. Magnetic field calibration

A permanent magnet is placed a few cm away from the diamond sample in order to apply a uniform magnetic field to the NV centers together with an electro-magnet.

To calibrate the magnetic field magnitude B, and its orientation θ with respect to the NV axis, we record Optically Detected Magnetic Resonance (ODMR) spectra....

D. Signal drift for levitating particles

Measurements on levitating diamonds have to be relatively short (few minutes at most) because of a slow drift on the particle orientation. The most likely origin of this drift is the loss of charges of the diamond due to photoionization by the laser, which changes the trapping conditions over time.

This drift is the reason why the photoluminescence scan on Fig.3 of the main text has a lower signal to noise ratio than the scan in Fig.1 of the main text, which was done on a

static diamond for a few hours.

E. Spin-mechanical detection

The microwave detuning is scanned in 2 MHz steps with a duration of 10 ms per points. During those 10ms, the diamond orientation has enough time to reach its equilibrium position and the spin torque effect can be observed. The average count-rate is about 1 MCounts/s.

F. PL detection

In these measurements, compared to [3], to detect the PL we use another detection channel that is more resilient to motion. We therefore do not need to detect prior to ring down.

III. PRINCIPLE OF THE MECHANICAL DETECTION

A. Origin of the magnetic torque and link to cross-relaxation

The magnetic torque responsible for the motion of the diamond fundamentally comes from the crystalline anisotropy of the NV centers and from the transverse field $B_\perp$ responsible for mixing the eigenstates in the stationary state. We will start by focusing on a single NV center.

As can be seen in Fig 4 b), when under green excitation and in the presence of an external magnetic field, the spins will acquire a magnetization $\gamma_e\langle\hat{\mathbf{S}}\rangle$ which, at the low magnetic fields (< 200 G) we are working at, will be oriented at a 90° angle from the NV axis : $\langle\hat{S}_z\rangle \approx 0$ and $\langle\hat{S}_\perp\rangle \neq 0$ This magnetization vanish when the magnetic field is aligned with the NV center since there is no longer a transverse field responsible for the mixing of the eigenstates.

The magnetization of the NV center is therefore not aligned with the magnetic field, except when the field is also at a 90° angle from the NV axis, which means that the magnetic torque $\mathbf{\Gamma} = \gamma_e\langle\hat{\mathbf{S}}\rangle \times \mathbf{B}$ will be non-zero everywhere except when the field is aligned with the center, or in the plane normal to the direction of the center. We can describe each NV center

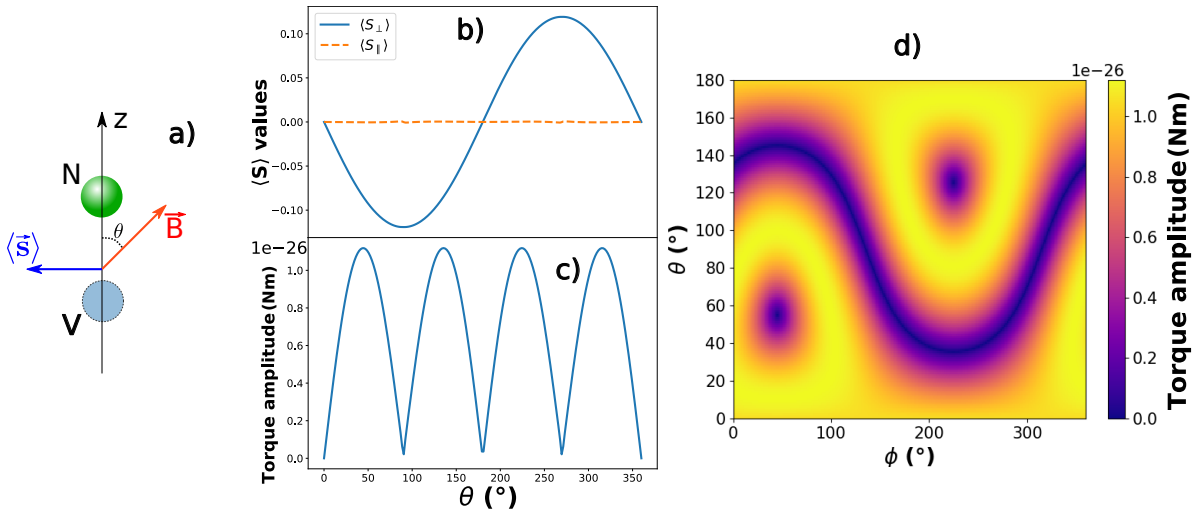

FIG. 4: **a)** Skecth of an NV center aligned in the **z** direction in the presence of an eternal magnetic field **B** forming an angle θ with the NV axis, and resulting magnetization $\gamma_e\langle\hat{\mathbf{S}}\rangle$ of the NV center **b)** Plotting of the longitudinal ($S_{\parallel}$ in dashed line) and transverse ($S_{\perp}$ in plain line) components of the spin operator average value, in $\hbar$ unit, as a function of θ and for a magnetic field amplitude $|\mathbf{B}| = 100$ G. **c)** Amplitude of the magnetic torque $\mathbf{\Gamma} = \gamma_e\langle\hat{\mathbf{S}}\rangle \times \mathbf{B}$ acting on a single spin as a function of θ for $|\mathbf{B}| = 100$ G. **d)** Amplitude of the same magnetic torque in the crystalline basis with θ and ϕ being the polar and azimuthal angle with respect to the [100] direction.

as a paramgnetic defect with the anisotropic magnetic suceptibility $\chi = \begin{pmatrix} -\chi_\perp & 0 & 0 \\ 0 & -\chi_\perp & 0 \\ 0 & 0 & 0 \end{pmatrix}$ in the $(\mathbf{x}, \mathbf{y}, \mathbf{z})$ basis where $\mathbf{z}$ is the orientation of the NV center.

The amplitude of the torque with respect to the magnetic field orientation (for an amplitude of 100 G) is represented in 1D in Fig 4 c) where we can see a behavior very close to $|sin(2\theta)|$, which is the formula (3) of the main text that we obtained through a perturbative approach. The same torque amplitude is represented in 2D in Fig 4 d) where the two dots correspond to the [111] direction, when the magnetic field is aligned with the centers, and the curvy line is the plane $[111]_\perp$. Important to note is the maximum torque value $1 \cdot 10^{-26}$ Nm for a single spin.

Fig 5 a) represents the same map but for four NV centers, one in each possible orientation. We can see that the maximum torque actually decreased to $3 \cdot 10^{-28}$ Nm even though we increased the number of NV centers by four. This is due to the directional averaging of the

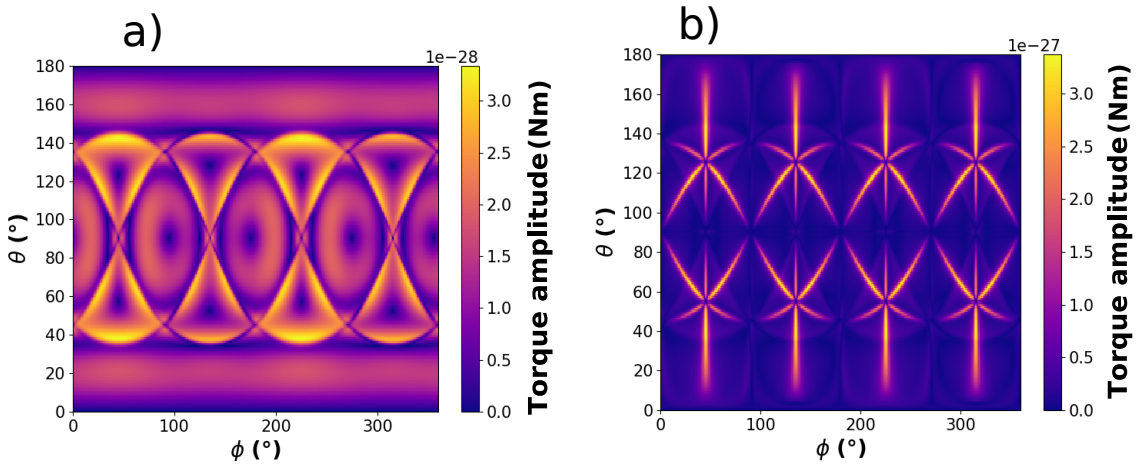

FIG. 5: Magnetic torque amplitude for 4 spins, one in each possible orientation, as a function of θ and ϕ, the polar and azimuthal angle with respect to the [100] direction. **a)** Not taking into account the CR between NV centers. **b)** Taking into account the CR between NV centers.

torque generated by the four centers. The torque per NV center is decreased by more than two order of magnitude when taking the directional averaging in consideration.

Finally, Fig 5 b) shows the same map, this time taking into account the modification of the spins lifetime due to cross-relaxations. There are two things to note here :

1. The maximum torque has increased by an order of magnitude compared to the previous case, up to $3 \cdot 10^{-27}$ Nm for four spins, or about 10^{-27} Nm per spin. Qualitatively, this is because cross-relaxation will lower the torque contribution of specific classes (the ones that get depolarized), meaning the the end result is closer to the single spin case (there is less directional averaging)

2. The change in magnetic torque is resonant, it happens only when different classes are brought to resonance (we can see in Fig 5 b) the $[110]_\perp$ planes that were drawn in Fig. 1), meaning that the change in signal when scanning a magnetic field will be much sharper.

B. Torque sensing with a levitating diamond

The way we can experimentally measure torques applied on a levitating diamond is by looking at the displacement of equilibrium caused by them. Here is a short model detailing

it :

We model the trap as a pure harmonical potential, both for the center of mass and for the rotational degrees of freedom of the diamond (REF ?), with trapping frequencies $\omega_T \approx (2\pi) \cdot 1$ kHz that we can experimentally measure. If we focus on a single rotational degree, we can write the torque generated by the trap as $\Gamma_T = -K(\theta - \theta_{eq})$, where $K = I\omega_t^2$ is the stiffness of the trap, I being the moment of inertia of the diamond.

The application of an external torque Γ_{ext} on the diamond will therefore shift the angular position at equilibrium in such a way that :

$$-K(\theta - \theta_{\text{eq}}) + \Gamma_{\text{ext}} = -K(\theta - \theta'_{\text{eq}})$$
$$\delta\theta = \theta'_{\text{eq}} - \theta_{\text{eq}} = \frac{\Gamma_{\text{ext}}}{K} = \frac{\Gamma_{\text{ext}}}{I\omega_t^2}$$

In our case, Γ_{ext} is the magnetic torque exerted by the NV^- spins on the diamond, such that we can write $\Gamma_{\text{ext}} = N_{NV}\langle\Gamma_{1\text{spin}}\rangle$ where $\langle\Gamma_{1\text{spin}}\rangle = \gamma_e\langle\hat{\mathbf{S}}\rangle \times \mathbf{B} \approx 10^{-27}$ Nm is the expected magnetic torque applied by one spin (see Fig 5).

By using the inertia moment formula of a sphere : $I = \frac{2}{5}mr^2$, we can then rewrite the angular displacement as

$$\delta\theta = \frac{\langle\Gamma_{1\text{spin}}\rangle n(NV^-)}{\frac{2}{5}m_C r^2\omega_T^2} \approx 10^{-4} rad$$

where $n(NV^-) \approx 5 \cdot 10^{-6}$ (5 ppm) is the number of NV centers per atoms in the crystal, $m_C \approx 2 \cdot 10^{-26}$ kg is the average weight of a carbon atom (we assume that the bulk of the diamond weight comes from carbon atoms), $r = 7.5$ μm is the typical radius of our diamonds and $\omega_T = 6.3 \cdot 10^3$ rad/s is the typical value of the trap angular frequency.

It should be noted that the main uncertainty comes here from the diamond size, which along the other uncertainties can change the expected result by an order of magnitude.

IV. CROSS-RELAXATION DETECTION FOR ANOTHER TYPE OF DEGENERACY

Similarly to Fig. 3 of the main text, we managed to mechanically detect another type of NV-NV resonance. Fig. 6b) shows the theoretical frequencies of the $|0\rangle \rightarrow |-1\rangle$ transitions for all four classes of NV and ESR spectra measured through the reflected laser light off the diamond for various magnetic field values. Unlike The experiment of the main text, this

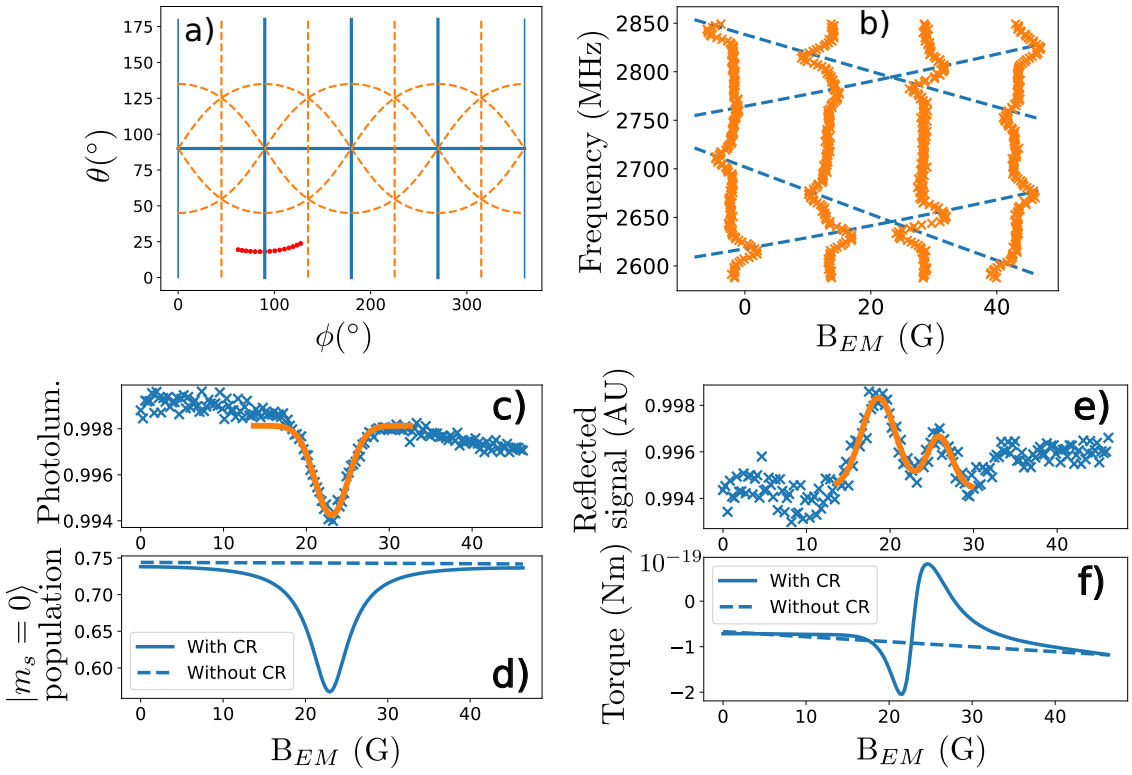

FIG. 6: Mechanical detection of a degeneracy in a $[100]_\perp$ plane.**a)** Path of the magnetic field along the scan (red dots) in the (θ, ϕ) basis with respect to the [100] direction. $[100]_\perp$ family of planes in plain blue lines, $[110]_\perp$ family of planes in orange dashed lines.**b)** Theoretical frequencies for the four $|0\rangle \rightarrow |-1\rangle$ transitions in dashed lines and experimental ESR spectra vertically. **c)** Photoluminescence of the NV centers as a function of the scanning magnetic field (blue crosses) and gaussian fit (orange line). **d)** Simulated population in $|m_s = 0\rangle$ for the stationary state with (plain) or without (dashed) taking into account the decrease of the T_1 induced by the cross-relaxations. **e)** Reflected signal off the diamond as a function of the scanning magnetic field (blue crosses) and double gaussian fit (orange line) **f)** Simulated torque applied by the spins on the diamond, with (plain) or without(dashed) taking into account the cross-relaxations.

time all four classes of NV are at resonance with another class at B=23 G, telling us that we are crossing a $[100]_\perp$ plane instead of a $[110]_\perp$ one, as can be seen on fig 6a)

Fig. 6c) shows the recorded photoluminescence of the NV centers during the magnetic field scan. As previously, we see a drop in the luminosity when the resonance occurs, that we fitted with a gaussian. The drop is slightly more pronounced in this case since all classes are depolarized, instead of only two in the previous experiment. This behavior is predicted

by the simulation of the $|m_s = 0\rangle$ population in the stationary state in Fig. 6d).

Fig. 6e) shows the signal of the reflected laser off the diamond, allowing us to measure angular displacement. This time we see a clear difference with the experiment of the main text, instead of a single drop centered on the resonance, we see two bumps on both sides of the resonance, fitted with two gaussians. This is in accordance with the simulated torque in Fig. 6f) where we can see a dispersive profile with an almost zero torque at the resonance. The reason we do not observe a change of sign in the experiment (with two positive bumps instead of a positive and a negative one) might be because of the strong non-linearity of our detection : if the signal initially correspond to a dark spot of the speckle, then a change in the motion of the diamond can only result in an increased signal. We also note a drop both in the predicted torque amplitude, and in the signal-to-noise ratio of the angular measurement compared to the single degeneracy case, implying a weaker effect.

Our physical interpretation of the angular signal we observe, as well as the dispersive profile of the torque is that in this case, for symmetry reason, the magnetic torque generated by the four classes of NV is not modified when we are exactly at resonance, since all four classes are affected identically. What happens when being near, but not at, resonance is that the classes will not be identically depolarized : looking at Fig. 6b), we can see that the two classes of higher frequency are always slightly closer to each other than the two classes of lower frequency (we can see the slope of the frequencies being a bit smaller for the two upper classes), resulting in a bit more depolarization for these two classes, except when they are exactly at resonance. This interpretation accounts both for the overall shape of the responses, and the comparatively weakness of the phenomenon.

V. SIMULATION DETAILS

In this part we will discuss the method used to simulate the average torque as well as the $|m_s = 0\rangle$ population of the stationary state. The numerical solving of the master equations was performed thanks to the Quantum Toolbox in Python (QuTiP) [4] [5].

In order to describe the dynamics of our spin ensemble, besides the spin Hamiltonian described in the first part, we introduce the incoherent optical pumping through the jump operators $\mathcal{L}_+ = \Gamma_l \left|0\right\rangle \left\langle +1\right|$ and $\mathcal{L}_- = \Gamma_l \left|0\right\rangle \left\langle -1\right|$, where $\Gamma_l \approx (2\pi)10\text{kHz}$ is the polarizing rate due to the laser.

We also introduce the usual T_1 jump operators $\mathcal{L}_i^j = \frac{1}{T_1} |i\rangle \langle j|$ where $|i,j\rangle = |0, \pm 1\rangle$

In order to describe the T_1 modification induced by the cross-relaxations, we use a phenomenological model where each class as its own T_1^i (i from 1 to 4) that depends on the energy levels of the other classes with the formula :

$$\frac{1}{T_1^i} = \frac{1}{T_1^0} + \sum_{j \neq i} \frac{1}{T_1^{dd}} e^{-\frac{(\nu_i - \nu_j)^2}{2(\sigma^{dd})^2}},$$

where ν_i and ν_j are the transition frequencies of the classes i and j (we are arbitrarily considering the $|0\rangle \rightarrow |-1\rangle$ transition here, since the resonance condition is the same for both transitions at the magnetic fields we are working at. This would not always be true for magnetic fields greater than 592 G[6]).

$\sigma^{dd} = 6$ MHz is the the dipolar interaction width, which we measured to be similar to the inhomogeneous broadening.

$T_1^0 = 1.03$ ms and $T_1^{dd} = 0.38$ ms were chosen to match the T_1 measured in Fig. 1 of the main text. We only focus on the T_1 without degeneracy and the one with a single degeneracy since our experiments will not have more than two classes at resonance at once. Our model is probably not suited to deal with triple our quadruple resonances.

Finally, according to previous measurements [7], only the $|0\rangle \langle \pm 1|$ and $|\pm 1\rangle \langle 0|$ (corresponding to a single quantum exchange in the dipole-dipole interaction) operators are modified by the cross-relaxations.

With this model in consideration, we can numerically solve the master equation and get the density matrix in the stationary state ρ_s. With ρ_s we can directly obtain the $|m_s = 0\rangle$ population, corresponding experimentally to the photoluminescence.

As for the torque, we use a semi-classical formula :

$$\mathbf{\Gamma} = N_0 \gamma_e \langle \hat{\mathbf{S}} \rangle \times \mathbf{B},$$

where $N_0 \approx 10^9$ is an estimate of the number of spins in our sample based on the average size and NV density of our diamonds, γ_e is the gyromagnetic ratio of the electron and $\langle \hat{\mathbf{S}} \rangle = \mathrm{Tr}(\rho_s \hat{\mathbf{S}})$ is the averaged spin vector in the stationary sate, averaged again on the four possible orientations of NV. This formula assumes that the spin dynamics is faster than the dynamics of the motion of the diamond, which is the case in our experiments.

In our plots in Fig. 6 and Fig. 3 of the main ext, we only represent one spatial component

(e.g. Γ_x) of the torque, but the three components behave similarly.

---

[1] T. Delord, P. Huillery, L. Schwab, L. Nicolas, L. Lecordier, and G. Hétet, Phys. Rev. Lett. **121**, 053602 (2018).

[2] T. Delord, Ph.D. thesis, École Normale Supérieure (2019).

[3] T. Delord, P. Huillery, L. Nicolas, and G. Hétet, Nature **580**, 56 (2020).

[4] J. R. Johansson, P. D. Nation, and F. Nori, Computer Physics Communications **183**, 1760 (2012).

[5] J. Johansson, Comp. Phys. Comm **184**, 1234 (????).

[6] E. van Oort and M. Glasbeek, Phys. Rev. B **40**, 6509 (1989), ISSN 0163-1829, number: 10, URL `https://link.aps.org/doi/10.1103/PhysRevB.40.6509`.

[7] J. Choi, S. Choi, G. Kucsko, P. C. Maurer, B. J. Shields, H. Sumiya, S. Onoda, J. Isoya, E. Demler, F. Jelezko, et al., Phys. Rev. Lett. **118**, 093601 (2017), ISSN 0031-9007, 1079-7114, number: 9, URL `https://link.aps.org/doi/10.1103/PhysRevLett.118.093601`.